Earth and Planetary Science Letters 337–338 (2012) 114–120

Contents lists available at SciVerse ScienceDirect

Earth and Planetary Science Letters

journal homepage: www.elsevier.com/locate/epsl

A new model of cosmogenic production of radiocarbon ^{14}C in the atmosphere

Gennady A. Kovaltsov [a], Alexander Mishev [b,c], Ilya G. Usoskin [b,d,*]

[a] Ioffe Physical-Technical Institute, St. Petersburg, Russia
[b] Sodankylä Geophysical Observatory (Oulu unit), University of Oulu, Finland
[c] Institute for Nuclear Research and Nuclear Energy, Bulgarian Academy of Sciences, 72 Tzarigradsko chaussee, 1784 Sofia, Bulgaria
[d] Department of Physical Sciences, University of Oulu, Finland

ARTICLE INFO

Article history:
Received 2 February 2012
Received in revised form
3 May 2012
Accepted 7 May 2012
Editor: B. Marty

Keywords:
cosmic rays
Earth's atmosphere
cosmogenic isotopes
radiocarbon ^{14}C

ABSTRACT

We present the results of full new calculation of radiocarbon ^{14}C production in the Earth atmosphere, using a numerical Monte-Carlo model. We provide, for the first time, a tabulated ^{14}C yield function for the energy of primary cosmic ray particles ranging from 0.1 to 1000 GeV/nucleon. We have calculated the global production rate of ^{14}C, which is 1.64 and 1.88 atoms/cm^2/s for the modern time and for the pre-industrial epoch, respectively. This is close to the values obtained from the carbon cycle reservoir inventory. We argue that earlier models overestimated the global ^{14}C production rate because of outdated spectra of cosmic ray heavier nuclei. The mean contribution of solar energetic particles to the global ^{14}C is calculated as about 0.25% for the modern epoch. Our model provides a new tool to calculate the ^{14}C production in the Earth's atmosphere, which can be applied, e.g., to reconstructions of solar activity in the past.

1. Introduction

Radiocarbon ^{14}C is a long-living (half-life about 5730 yr) radioactive nuclide produced mostly by cosmic rays in the Earth's atmosphere. Soon after production, it gets oxidized to $^{14}CO_2$ and in the gaseous form takes part in the complex global carbon cycle (Bolin et al., 1979). Radiocarbon is important not only because it is used for dating in many applications (e.g., Dorman, 2004; Kromer, 2009), but also because it forms a primary method of paleo-reconstructions of solar activity on the millennial time scales (e.g., Stuiver and Quay, 1980; Stuiver and Braziunas, 1989; Bard et al., 1997; Muscheler et al., 2007). An essential part of the solar activity reconstruction from radiocarbon data is computation of ^{14}C production by cosmic rays in the Earth's atmosphere. First such computations were performed in the 1960–1970s (e.g., Lingenfelter, 1963; Lingenfelter and Ramaty, 1970; Light et al., 1973; O'Brien, 1979) and were based on simplified numerical or semi-empirical methods. Later, full Monte-Carlo simulations of the cosmic-ray induced atmospheric cascade had been performed (Masarik and Beer, 1999, 2009). Most of the earlier models, including O'Brien (1979) and Masarik and Beer (1999) deal with a prescribed functional shape of the galactic cosmic ray spectrum, which makes it impossible to be applied to other types of cosmic ray spectra, e.g., solar energetic particles, supernova explosions, etc. A flexible approach includes calculation of the yield function (the number of cosmogenic nuclei produced in the atmosphere by the primary cosmic rays of the given type with the fixed energy and unit intensity outside the atmosphere), which can be convoluted with any given energy spectrum of the primary cosmic rays (e.g., Webber and Higbie, 2003; Webber et al., 2007; Usoskin and Kovaltsov, 2008; Kovaltsov and Usoskin, 2010). This approach can be directly applied to, e.g., a problem of the signatures of extreme solar energetic particle events in the cosmogenic nuclide data, which is actively discussed (e.g., Usoskin et al., 2006; Hudson, 2010; LaViolette, 2011). Some earlier models (Lingenfelter, 1963; Castagnoli and Lal, 1980) provide the ^{14}C yield function however it is limited in energy. Moreover, different models give results, which differ by up to 50% from each other, leading to large uncertainty in the global ^{14}C production rate. Therefore, the present status is that models providing the yield function are 30–50 yr old and have large uncertainties.

In addition, there is a systematic discrepancy between the results of theoretical models for the ^{14}C production and the global average ^{14}C production rate obtained from direct measurements of the specific $^{14}CO_2$ activity in the atmosphere and from the carbon cycle reservoir inventory. While earlier production models predict that the global average pre-industrial production rate should be 1.9–2.5 atoms/cm^2/s, estimates from the carbon cycle inventory give systematically lower values ranging between 1.6 and 1.8 atoms/cm^2/s (Lingenfelter, 1963; Lal and Suess,

* Corresponding author at: Sodankylä Geophysical Observatory (Oulu unit), University of Oulu, Finland. Tel.: +358 50 3441247; fax: +358 8 5531390.
E-mail address: ilya.usoskin@oulu.fi (I.G. Usoskin).

0012-821X/$ - see front matter © 2012 Elsevier B.V. All rights reserved.
http://dx.doi.org/10.1016/j.epsl.2012.05.036

1968; Damon and Sternberg, 1989; O'Brien et al., 1991; Goslar, 2001; Dorman, 2004). This discrepancy is known since long (Lingenfelter, 1963) but is yet unresolved (Goslar, 2001).

In this work we redo all the detailed Monte-Carlo computations of the cosmic-ray induced atmospheric cascade and the production of ^{14}C in the atmosphere to resolve the problems mentioned above. In Section 2 we describe the numerical model and calculation of the radiocarbon production. In Section 3 we compare the obtained results with earlier models. In Section 4 we apply the model to calculate the ^{14}C production by galactic cosmic rays and solar energetic particle events for the last solar cycle. Conclusions are presented in Section 5.

2. Calculation of the ^{14}C production

Energetic primary cosmic ray particles, when entering the atmosphere, collide with nuclei of the atmospheric gases initiating a complicated nucleonic cascade (also called shower). Here we are interested primarily in secondary neutrons whose distribution in the atmosphere varies with altitude, latitude, atmospheric state and solar activity. Neutrons are produced in the atmosphere through multiple reactions including high-energy direct reactions, low-energy compound nucleus reactions and evaporation of neutrons from the final equilibrium state. Most of the neutrons with energy below 10 MeV are produced as an evaporation product of excited nuclei, while high-energy neutrons originate as knock-on neutrons in collisions or in charge exchange reactions of high-energy protons. While knock-on neutrons are mainly emitted in the forward direction (viz. downwards), evaporated neutrons of lower energy are nearly isotropic. Radiocarbon ^{14}C is a by-product of the nucleonic cascade, with the main channel being through capture of secondary neutrons by nitrogen: N14(n,p)C14. Other channels (e.g., via spallation reactions) contribute negligibly, but are also considered here.

We have performed a full Monte-Carlo simulation of the nucleonic component of the cosmic ray induced atmospheric cascade, using the Planetocosmic code (Desorgher et al., 2005) based on GEANT-4 toolkit for the passage of particles through matter (Geant4 Collaboration, 2003) (see details in Appendix). The secondary particles were tracked through the atmosphere until they undergo reactions with an air nucleus, exit the atmosphere or decay. In particular, secondary neutrons were traced down to epi-thermal energy. Simulations are computationally intensive. Simulations of single energies (ranging from 0.1 to 1000 GeV/nucleon) were conducted, to determine the resulting flux of secondary neutrons. Since the calculations require very large computational time to keep the statistical significance of the results for low energies, we applied an analytical approach for atmospheric neutrons with energy below 10 eV (see details in Appendix). Cross-sections have been adopted from the Experimental Nuclear Reaction Database (EXFOR/CSISRS) http://www.nndc.bnl.gov/exfor/exfor00.htm. The number of simulated cascades induced by primary CR particles was chosen as 10^5-10^6 to keep the statistical stability of the results at a reasonable computational time. Computations were carried out separately for primary protons and α-particles. Because of the similar rigidity/energy ratio, nuclei with $Z>2$ were considered as effectively α-particles with the scaled number of nucleons (cf. Usoskin and Kovaltsov, 2008).

As the main result of these detailed computations we calculated the ^{14}C yield function. The yield functions for primary protons and α-particles are tabulated in Table 1 and shown in Fig. 1 (the energy range above 100 GeV/nucleon is not shown). Note that the yields (per nucleon with the same energy) are identical for protons and α-particle, viz. an α-particle is identical to four protons, at energies above 10 GeV/nucleon. Details of the computations are given in Appendix A. All further calculations are made using these yield functions.

In order to compute the ^{14}C production q in the atmosphere at a certain place and conditions/time, one can use the following method:

$$q(t)=\sum_i \int_{E_{ic}}^{\infty} Y_i(E)J_i(E,t)\,dE, \tag{1}$$

where E is the particle's kinetic energy per nucleon, J_i is the spectrum of primary particles of type i on the top of the atmosphere, E_{ic} in GeV/nucleon is the kinetic energy per nucleon corresponding to the local geomagnetic rigidity cutoff P_c in GV

$$P_c=\frac{A_i}{Z_i}\sqrt{E_{ic}\,(E_{ic}+2E_r)}, \tag{2}$$

where $E_r=0.938$ GeV/nucleon is the proton's rest mass. Summation is over different types of the primary cosmic ray nuclei with charge Z_i and mass A_i numbers. The local geomagnetic rigidity cutoff is roughly defined via the geomagnetic latitude λ_G of the location as following (Elsasser et al., 1956):

$$P_c\,[\mathrm{GV}]=1.9\cdot M\cdot\cos^4\lambda_G, \tag{3}$$

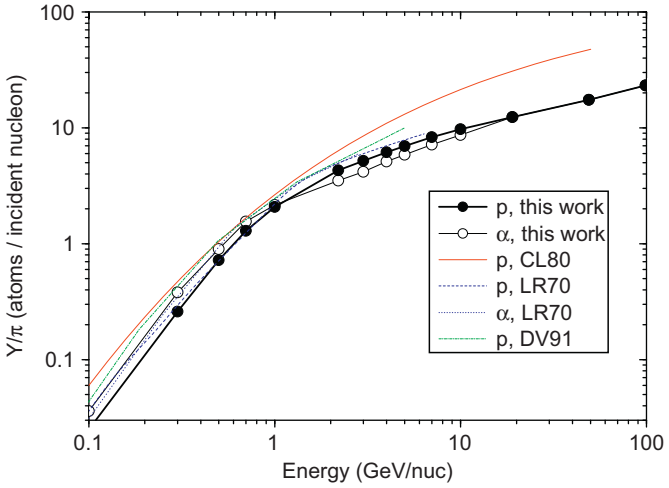

Fig. 1. Yield function Y/π of ^{14}C production in the Earth's atmosphere by primary cosmic ray protons and α-particles (as denoted by "p" and "α" in the legend, respectively) with given energy per nucleon. Different curves correspond to the present work (Table 1) and earlier models Castagnoli and Lal (1980, CL80), Lingenfelter and Ramaty (1970, LR70) and Dergachev and Veksler (1991, DV91), as denoted in the legend.

Table 1
Normalized yield functions Y_p/π and Y_α/π of the atmospheric columnar ^{14}C production (in atoms sr) by a nucleon of primary cosmic protons and α-particles, respectively, with the energy given in GeV/nucleon. For energy above 20 GeV/nucleon, an α-particle is considered to be identical to four protons.

E (GeV/nucleon)	0.1	0.3	0.5	0.7	1	3	7	10	19	49	99	499	999
Proton	0.025	0.26	0.72	1.29	2.07	5.19	8.32	9.72	12.40	17.45	23.24	48.30	72.73
α/4	0.036	0.38	0.89	1.55	2.16	4.18	7.17	8.67	12.40	17.45	23.24	48.30	72.73

where M is the dipole moment in units of [10^{22} A m^2] of the Earth's magnetic field. Although this approximation may slightly $\leq 2\%$ overestimate the ^{14}C production (O'Brien, 2008), it is sufficient to study the global cosmic ray flux (Dorman, 2009; Clem et al., 1997). The global production Q of radiocarbon is defined as the spatial global average of the local production q (both quantities give the number of ^{14}C nuclei produced per second per cm^2 of the Earth's surface). For the isotropic flux of primary particles in the interplanetary space (the level of anisotropy for galactic cosmic rays is usually smaller than 1%) the global production can be written as

$$Q(t) = \sum_i \int_0^\infty Y_i(E) J_i(E,t)(1-f(E))\, dE, \tag{4}$$

where the function

$$f(E) = \begin{cases} \sqrt{1-\sqrt{P(E)/(1.9\cdot M)}} & \text{if } P \leq 1.9\cdot M, \\ 0 & \text{if } P > 1.9\cdot M \end{cases} \tag{5}$$

corresponds to $\sin(\lambda_G)$ and accounts for the spatial average with the effect of the geomagnetic cutoff.

Substituting any particular particle spectrum J_i into Eq. (4) one can evaluate the ^{14}C production rate for different populations of cosmic rays, e.g., galactic cosmic rays (GCRs), solar energetic particles (SEPs), or more exotic sources like a nearby supernova explosion.

First we consider the main source of ^{14}C, GCR modulated by the solar activity, using the standard approach. The energy spectrum of GCR particles of type i at 1 AU, J_i, is defined by the local interstellar spectrum (LIS), $J_{LIS,i}$, and the modulation potential ϕ as (see the formalism in Usoskin et al., 2005)

$$J_i(E,\phi) = J_{LIS,i}(E+\Phi_i)\frac{(E)(E+2E_r)}{(E+\Phi_i)(E+\Phi_i+2E_r)}, \tag{6}$$

where $\Phi_i = (eZ_i/A_i)\phi$. The modulation potential ϕ is the variable related to solar activity, that parameterizes the shape of the modulated GCR spectrum. The fixed function $J_{LIS}(T)$ is not exactly known and may affect the absolute value of ϕ (e.g., Usoskin et al., 2005; Webber and Higbie, 2009; Herbst et al., 2010; O'Brien, 2010). Thus, the exact model of LIS must be specified together with the values of ϕ. Here we use, as earlier, the proton LIS in the form (Burger et al., 2000; Usoskin et al., 2005)

$$J_{LIS}(E) = \frac{1.9\times 10^4 \cdot P(E)^{-2.78}}{1+0.4866\, P(E)^{-2.51}}, \tag{7}$$

where $P(E) = \sqrt{E(E+2E_r)}$, J and E are expressed in units of particles/(m^2 sr s GeV/nucleon) and in GeV/nucleon, respectively. Here we consider two species of GCR separately: protons and heavier species, the latter including all particles with $Z>1$ as α-particles with $Z/A = 0.5$ scaled by the number of nucleons. Heavier species should be treated separately as they are modulated in the heliosphere and Earth's magnetosphere differently, compared to protons because of the different Z/A ratio. Here we consider the nucleonic ratio of heavier particles (including α-particles) to protons in the interstellar medium as 0.3 (Webber and Higbie, 2003; Nakamura et al., 2010).

The global ^{14}C production Q by GCR depends on two parameters, the solar magnetic activity quantified via the modulation potential ϕ and the Earth's geomagnetic field (its dipole moment M). The dependence is shown in the upper panel of Fig. 2. One can see that both parameters are equally important, and the knowledge of the geomagnetic field is very important (Snowball and Muscheler, 2007). In the lower panel, three cuts of the upper panel are shown to illustrate the effect of solar activity on Q, for the fixed geomagnetic field, corresponding to the modern conditions $M = 7.8\times 10^{22}$ A m^2, as well as maximum (10^{23} A m^2) and minimum (6×10^{22} A m^2) dipole strength over the last 10 millennia of the Holocene (Korte et al., 2011). The response of Q to changes of the geomagnetic field during the Holocene is within $\pm 15\%$. However, the global ^{14}C would be nearly doubled during an inversion of the geomagnetic field (viz. $M\to 0$). The modulation potential ϕ varies between about 300 and 1500 MV within a modern high solar cycle (Usoskin et al., 2011), and can be as low as about 100 MV during the Maunder minimum (McCracken et al., 2004; Usoskin et al., 2007; Steinhilber et al., 2008). Thus, changes of the solar modulation can also lead to a factor of 2–3 variability on the global ^{14}C production rate.

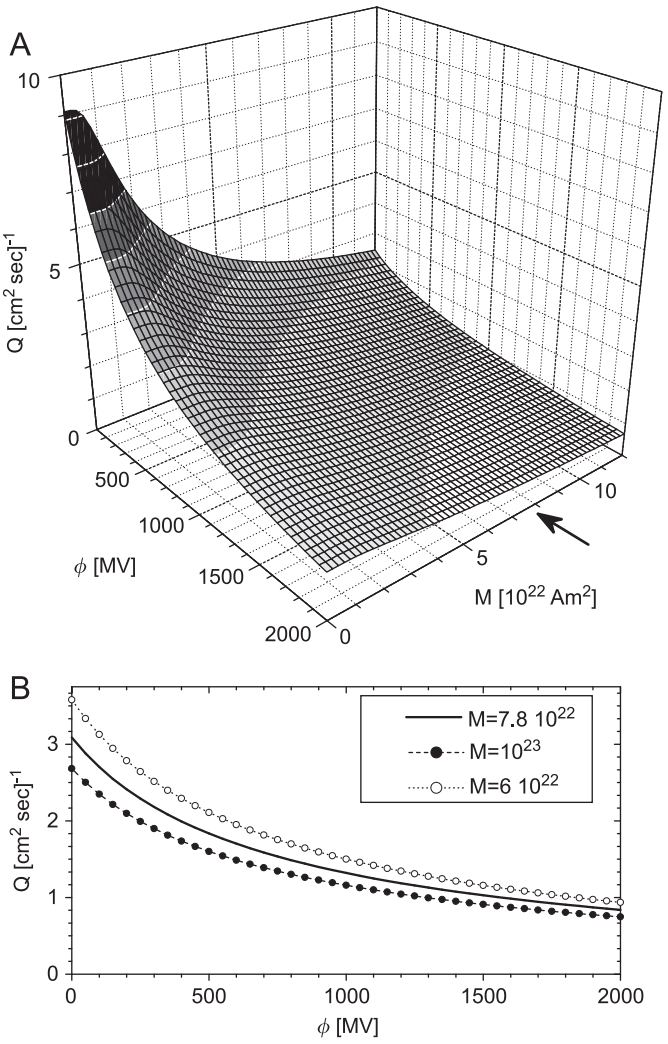

Fig. 2. The global production of ^{14}C as function of the modulation potential ϕ and the geomagnetic dipole moment M. The present value of $M = 7.8\times 10^{22}$ A m^2 is indicated by the thick arrow. The lower panel shows three cross-sections of the upper panel corresponding to the present value as well as to the maximum and minimum values of M over the past millennia, as indicated in the legend. Digital table for this plot is available at electronic supplement for this paper.

Next we investigated the sensitivity of Q to the energy of GCR. In Fig. 3 we show the relative cumulative production of ^{14}C, viz. the fraction of the total production caused by primary cosmic rays with energy below the given value E, as a function of E for different conditions. Often the median energy (the energy which halves the production) is used as a characteristic energy (e.g., Lockwood and Webber, 1996), which is the crossing of the curves in Fig. 3 with the horizontal dashed line. One can see that the median energy of ^{14}C production slightly changes with the level of solar activity, varying between 4 and 10 GeV/nucleon corresponding to the Maunder minimum and the maximum of a strong

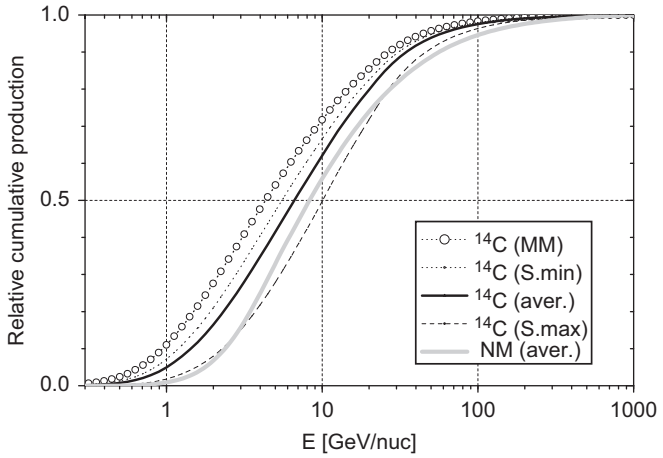

Fig. 3. Relative cumulative production of ^{14}C (fraction of the total production) as a function of the primary cosmic ray energy for different conditions: average solar activity (solid "aver." curve), solar maximum ($\phi = 1200$ MV, dashed "S.max" curve), solar minimum ($\phi = 300$ MV, dotted "S.min" curve), Maunder minimum ($\phi = 100$ MV, circled "MM" curve). The thick gray curve corresponds to a polar sea-level neutron monitor. All curves are shown for the modern Earth magnetic field.

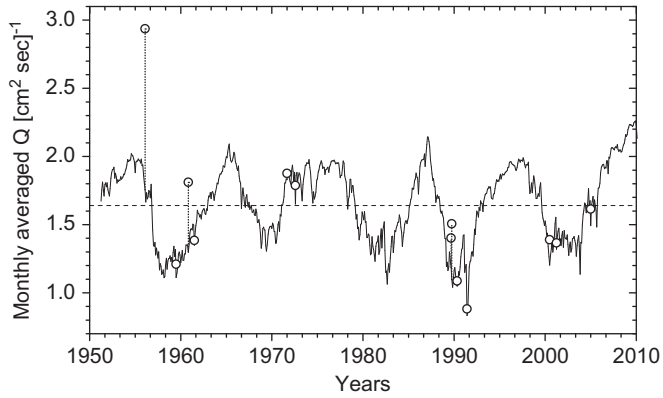

Fig. 4. Monthly averaged global production rates of ^{14}C since 1951 calculated using cosmic rays data from the world network of neutron monitors and our calculated yield function. Open circles correspond to months with major solar energetic particle events.

solar cycle, respectively. The sensitivity of Q to the energy of GCR is close to that of a sea-level polar neutron monitor (cf. Beer, 2000). Slightly different shape of the neutron monitor cumulative response is due to the fact that it is ground-based while ^{14}C is produced in the entire atmosphere.

As an example, we calculated the ^{14}C production predicted by the model for the last 60 yr (see Fig. 4) using the GCR modulation, reconstructed from the ground-based network of neutron monitors (Usoskin et al., 2011), and IGRF (International Geomagnetic Reference Field—http://www.ngdc.noaa.gov/IAGA/vmod/igrf.html) model of the Earth's magnetic field. The mean radiocarbon production for that period (1951–2010) is $Q = 1.64$ atom/cm^2/s, with the variability by a factor of two between 1.1 (in 1990 solar maximum) and 2.2 (in 2010 solar minimum) atom/cm^2/s.

The mean ^{14}C production for the pre-industrial period (1750–1900) calculated using the GCR modulation reconstruction by Alanko-Huotari et al. (2007) and paleomagnetic data by Korte et al. (2011) is 1.88 atom/cm^2/s which is essentially lower than those reported in earlier works (1.9–2.5 atom/cm^2/s) and closer to the values obtained from the carbon cycle inventory (1.6–1.8 atom/cm^2/s)—see Introduction. These values can be further $\approx 2\%$ lower because of the used geomagnetic cutoff approach (O'Brien, 2008).

3. Comparison with earlier models

In Fig. 1 we compare our present results with the yield functions calculated earlier (see the figure caption for references). Our results are consistent with most of the earlier calculations (LR70 and DV91) within 10–20%. The CL80 yield function is not independently calculated but modified from LR70. While it is formally given for protons it effectively includes also α-particles via scaling, thus being systematically higher than the other yield functions. Note that all the earlier computations of the yield function were limited in energy so that the upper considered energy of primary cosmic rays was from several to 50 GeV/nucleon. On the other hand, contribution of higher energy cosmic rays is significant and may reach half of the total ^{14}C production (see Fig. 3). Here we present, for the first time, the ^{14}C yield function calculated up to TeV/nucleon energy. Contribution from the higher energies is negligible because of the steep spectrum of GCR.

Next we perform a more detailed comparison with the most recent ^{14}C production model by Masarik and Beer (2009, MB09), who also used a GEANT-4 Monte-Carlo simulation tool. Since MB09 did not calculate the yield function, we use another way of comparison, via computing the global averaged ^{14}C production rate, as illustrated in Fig. 5. Our present result (black curve Q) in the figure is systematically lower than that given by MB09 (big dots) by 25–30%. We suspect that the discrepancy arises from that Masarik and Beer (2009) calculated the ^{14}C production for a prescribed GCR spectrum in the form given by Garcia-Munoz et al. (1975) and Castagnoli and Lal (1980), which is different from the spectrum we use here (adopted from Usoskin et al., 2005; Herbst et al., 2010). Thus, in order to compare our results with those of MB09, we repeat our computations based on Eq. (1) to compute the global production Q^* but using the same spectrum as MB09. The result for Q^* is shown by the gray curves in Fig. 5.

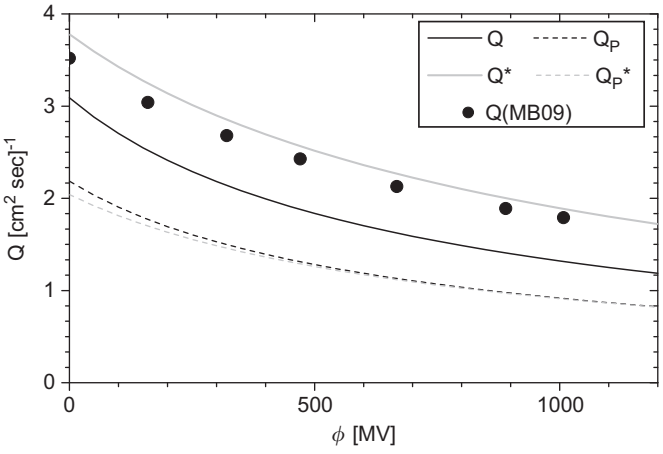

Fig. 5. Comparison of the global ^{14}C production rates, computed by different models as a function of the modulation potential for the modern geomagnetic field. Big dots correspond to the original results by Masarik and Beer (2009). Curves are computed using our calculated yield function (Table 1) and applying different cosmic rays spectra. Black curves (Q values) are calculated using the present results, while gray curves (Q* values) are calculated using our yield function but GCR spectra as used by Masarik and Beer (2009). Solid and dashed lines correspond to the total production and to production only by primary protons, respectively.

The overall agreement is within 5% but Q^* value is systematically higher than that of MB09. The 5% difference can be related to the slightly different numerical scheme and also to the fact that MB09 treated an α-particle as four protons while we simulated them straightforwardly. In addition, the way of considering the geomagnetic shielding by MB09 is simplified (scaling) compared to our consideration (direct computations). We also compared the proton contributions (two dashed curves in Fig. 5) to Q for the GCR spectrum discussed here (Eq. (6)) and that used in MB09. The curves are nearly identical, suggesting that the difference in the used proton spectra is small and cannot be a cause for the observed systematic difference. We however notice a great difference between the α (and heavier) particle spectra used here and in MB09. MB09 assumed 12% for α and 1% for heavier particle fraction in LIS (leading to ≈0.64 nucleonic ratio between heavier species to protons in GCR) based on the data from Simpson (1983). On the other hand, modern measurements (e.g., AMS, PAMELA) suggest that α-particles above 10 GeV/nucleon contribute 5–6% (in particle number) to LIS of GCR leading to the nucleonic fraction of heavier species to protons of the order of 0.25–0.3 outside the heliosphere (e.g, Alcaraz et al. 2000a,b; Adriani et al., 2011; Webber and Higbie, 2003; Nakamura et al., 2010), viz. half of that assumed by MB09. Therefore, while we agree with MB09 in calculations of proton contribution into Q, they overestimate ^{14}C production by heavier species of GCR, using outdated spectra. This explains why the earlier results by MB99 and MB09 of ^{14}C production are systematically higher than our present result.

Next we compare predictions of our model with other models' results for specific periods of time as shown in Fig. 6 (exact data sets used are mentioned in the figure caption). One can see that our model predicts systematically lower production rates than most of other models, except of the model by O'Brien (1979) and O'Brien et al. (1991). On the other hand, our yield function is generally consistent with others (Fig. 1), indicating that the difference must be related to the treatment of incoming GCR particle spectra and/or geomagnetic shielding and not to the atmospheric cascade simulations. Models other than that by O'Brien (1979) were based on theoretical calculations and included outdated overestimated abundance of α-particles, which explains the difference as discussed above. Therefore, we conclude that our model more correctly calculates the ^{14}C production as it agrees with the empirically based models.

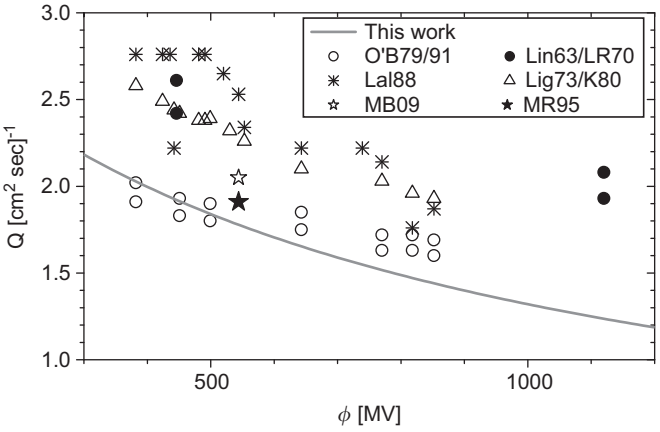

Fig. 6. Global ^{14}C production as function of the modulation potential ϕ as defined in Usoskin et al. (2011). The thick gray curve presents the present work's results. Symbols correspond to earlier works: O'B79/91 (Table 7 in O'Brien, 1979; O'Brien et al., 1991); Lin63/LR70 (Table 1 in Lingenfelter, 1963; Lingenfelter and Ramaty, 1970); Lal88 (Tables I and III in Lal, 1988); Lig73 (Table 6 in Light et al., 1973), K80 (Table 1 in Korff and Mendell, 1980); MB09 (Table 3 in Masarik and Beer, 2009); MR95 (Table 1 in Masarik and Reedy, 1995).

4. ^{14}C production by solar energetic particles

We also calculated production of radiocarbon by solar energetic particles (SEPs), because presently there is a wide range of the results (e.g., Lingenfelter and Ramaty, 1970; Usoskin et al., 2006; Hudson, 2010; LaViolette, 2011). Here we compute the expected production of ^{14}C by the major known SEP events since 1951, using our calculated yield function (Table 1) and SEP event-integrated spectra as reconstructed by Tylka and Dietrich (2009). The corresponding production rate is shown by big open dots in Fig. 4 reduced to the monthly mean values. One can see that only a few SEP events can produce significant enhancements in ^{14}C production (≈70% in the monthly mean for the SEP event of 23-February-1956, 40% for 12-November-1960, 35% for two events in October-1989 and ≈20% for 29-September-1989). However, when applied to the annual time scale (the standard tree-ring time resolution), it gives only a few percent effect for years of maximum solar activity and about 0.25% of the total contribution over the considered period. This is consistent with the earlier results by Lingenfelter and Ramaty (1970) (1.1% mean contribution of SEP into the global ^{14}C production for 1954–1965, our model for the same period gives 0.8%) and by Usoskin et al. (2006) (0.2% for 1955–2005). Note that MB09, however, gives much smaller value of 0.02% for the SEP contribution to the global mean ^{14}C production, which is probably caused by the neglect of the atmospheric cascade (and thus neutron capture channel) caused by SEPs (cf. Masarik and Reedy, 1995).

5. Conclusions

- We have performed full new calculation, based on a detailed Monte-Carlo simulation of the atmospheric cascade by a GEANT-4 tool PLANETOCOSMICS, of the ^{14}C yield function. This is the first new calculation of the yield function since 1960–1970s, using modern techniques and methods, and the yield function is, for the first time ever, directly computed up to the energy of 1000 GeV/nucleon (earlier models were limited to a few tens GeV/nucleon and extrapolated to higher energies). Our newly computed yield function gives the results which are in good agreement with O'Brien (1979) and consistent with most of the earlier models, within 10–20%.
- We have calculated, using the new model and improved spectra of cosmic rays, the global production of ^{14}C, which appears to be significantly lower than earlier estimates and closer to the values obtained from the carbon cycle inventory. The calculated modern global production rate is 1.64 atom/cm^2/s, and the pre-industrial rate (1750–1900 AD) is 1.88 atom/g/cm^2, which is essentially lower than earlier estimates of 2–2.5 atom/cm^2/s.
- We explain that the earlier models (including a recent model by Masarik and Beer, 2009) overestimate the contribution of α-particle and heavier GCR species to the ^{14}C production, because of the use of outdated spectra.
- We have calculated, on the basis of the new model, contribution to the global ^{14}C production by SEP events, using updated energy spectra reconstructions by Tylka and Dietrich (2009). The mean contribution of the SEPs for the last 50 yr is estimated to be ≈0.25% of the total production.
- The present model provides an improved tool to calculate the ^{14}C production in the Earth's atmosphere. Using the absolutely dated ^{14}C calibration curve (Reimer et al., 2009), one can reconstruct the variability of cosmic rays in the past (e.g., Solanki et al., 2004) which, along with other long-term solar proxies has applications to paleoastrophysics, paleomagnetism and paleoclimatology (e.g., Beer et al., 2012).

Acknowledgments

This work uses results obtained in research funded from the European Union's Seventh Framework Programme (FP7/2007-2013) under grant agreement no 262773 (SEPServer). The High-Energy Division of Institute for Nuclear Research and Nuclear Energy—Bulgarian Academy of Sciences is acknowledged for the given computational time. GAK was partly supported by the Program No. 22 of presidium RAS. University of Oulu and the Academy of Finland are acknowledged for partial support.

Appendix A. Details of numerical computations

Numerical computations were done using the GEANT-based Monte-Carlo simulation tool Planetocosmics (Desorgher et al., 2005), which traces the atmospheric cascade induced by the primary cosmic ray particles in full detail, including the distribution of secondary particles. The Planetocosmics code has been recently verified (Usoskin et al., 2009) to agree within $\approx 10\%$ with another commonly used Monte-Carlo package CORSIKA (Heck et al., 1998), in the sense of energy deposition in the atmosphere. The code simulates interactions and decays of various particles in the atmosphere in a wide range of energy. For the computations, we applied a realistic spherical atmospheric model NRMLSISE-00 (Hedin, 1991; Picone et al., 2002). The QGSP_BIC_HP hadron interaction model has been applied with the standard electromagnetic interaction model.

As an input for the simulations we used primary particles with fixed energy that impinge upon the top of the atmosphere at the random angle isotropically from the 2π solid angle. All computations were normalized per one such simulated particle. From the simulations we obtained the sum of secondary neutrons with energy within the ΔE energy bin centered at the energy E_n, crossing a given horizontal level (atmospheric depth X g/cm^2), weighted with $|1/\cos\theta|$ (where θ is the zenith angle) to account for the geometrical factor, and divided by the energy bin width ΔE. This corresponds to the flux of secondary neutron with given energy $F(E_n,X)$ across a horizontal unit area, for the unit flux of primary cosmic rays on the top of the atmosphere. On the other hand, for quasi-stationary flux of neutrons this can be expressed as

$$F(E_n,X) \equiv n_n(E_n,X)v_n(E_n), \tag{A.1}$$

where n_n and v_n are the concentration (in [MeV cm^3]$^{-1}$) and velocity of neutrons with energy E_n at the atmospheric depth level X. Let us denote the integral columnar flux as

$$I(E_n) = \int_0^{X_m} F(E_n,X)\, dX, \tag{A.2}$$

where $X_m = 1033$ g/cm^2 is the total thickness of the atmosphere. Since our direct computations were performed down to energy of neutrons $E_1 = 10$ eV, we first computed the production of ^{14}C by these super-thermal neutrons

$$G_1 = \sum_j \int_h \left(\int_{E1}^{\infty} F(E_n,X) n_j(h) \sigma_j(E_n)\, dE_n \right) dh, \tag{A.3}$$

where the outer integral is taken over the atmospheric height h, the concentration of target nuclei $n_j(h)$ is defined as a product of the air density ρ and the content of the nuclei in a gram of air κ_j, $n_j(h) = \rho(h)\kappa_j$; $\sigma_j(E)$ is the cross-section of the corresponding reaction, and $dX = \rho(h)\, dh$, and summation is over target nuclei of different type (nitrogen $\kappa_N = 3.225 \times 10^{22}$ atom/g; oxygen $\kappa_O = 8.672 \times 10^{21}$ atom/g; argon $\kappa_{Ar} = 1.94 \times 10^{20}$ atom/g, we also accounted for the isotopic distribution within these groups). Eqs. (A.3) and (A.2) can be transformed so that

$$G_1 = \sum_j \kappa_j \int_{E1}^{\infty} I(E_n)\sigma_j(E_n)\, dE_n. \tag{A.4}$$

All the cross-sections, used here, have been adopted from the Experimental Nuclear Reaction Database (EXFOR/CSISRS) http://www.nndc.bnl.gov/exfor/exfor00.htm.

We note that all the processes related to leakage of neutrons from the atmosphere (to the space or to soil) as well as their decay are accounted for in the direct simulation.

Monte-Carlo simulations require extensive computational time in order to trace neutrons to thermal energy, thus compromising the statistical robustness of the results. On the other hand, the fate of 10 eV neutrons can be easily modeled theoretically, because of the simplicity of the processes involved, which allows us to save computational time and improve accuracy of the computations. The main process affecting epi-thermal neutrons in air is potential elastic scattering on N and O nuclei making neutrons to lose energy. After each elastic scattering, a neutron has a uniform distribution of energy (in the laboratory frame) between its energy before the scattering E_n and αE_n (e.g., Fermi, 2010, Chapter 7.2). Here

$$\alpha = \frac{(A-1)^2}{(A+1)^2}, \tag{A.5}$$

where A is the mass number of the target nucleus. Then the probability for a neutron with the energy E_n (if $E_1 \le E_n < E_1/\alpha$) before elastic scattering on a nuclei j to have energy E after the scattering so that $E < E_1$ is $(E_1 - \alpha_j E_n)/(E_n(1-\alpha_j))$. Accordingly the "flux" (in the energy domain) of neutrons crossing the energy boundary E_1 to (epi)thermal energies can be calculated as

$$N = \sum_j \int_h \int_{E_1}^{E_1/\alpha_j} F(E_n,X) n_j(X) \sigma_{el,j}(E_n) \frac{E_1 - \alpha_j E_n}{E_n(1-\alpha_j)}\, dE_n\, dh \tag{A.6}$$

or, using Eq. (A.2) as

$$N = \sum_j \kappa_j \int_{E_1}^{E_1/\alpha_j} I(E_n)\sigma_{el,j}(E_n) \frac{E_1 - \alpha_j E_n}{E_n(1-\alpha_j)} dE_n. \tag{A.7}$$

Reactions involving neutrons are: (1) N14(n,p)C14; (2) O17(n, α) C14; (3) N14(n, γ)N15; (4) O16(n, γ)O17; (5) O18(n, γ)O19 and (6) Ar40(n, γ)Ar41. Note that only reactions (1) and (2) lead to production of ^{14}C while others simply provide a sink for neutrons. Cross-sections of neutron capture in all these reactions for energies below 10 eV can be expressed as

$$\sigma_j = \frac{B_j}{v_n(E_n)}, \tag{A.8}$$

where B_j is a constant. Accordingly, the ^{14}C production by these neutrons can be calculated as

$$G_2 = N \frac{B_1 \cdot \kappa_{N14} + B_2 \cdot \kappa_{O17}}{\sum_j B_j \cdot \kappa_j}. \tag{A.9}$$

The bulk of radiocarbon ^{14}C is produced via reaction (1) and about 0.001% in reaction (2). This is the main channel (95.8%) of the neutron sink. We have also considered leakage of neutrons from the upper atmospheric layers and decay of neutrons during their thermalization. These processes appear to be unimportant. In addition, we also computed possible contribution of secondary and primary protons to ^{14}C production via spallation reactions (e.g., O16(p,X)C14). These reactions are responsible for a negligible contribution to the total production.

Then the final production of ^{14}C in the atmosphere by secondary neutrons corresponding to the primary cosmic ray particle with given energy is the sum of G_1 and G_2 and forms a point in the yield function Y/π.

Appendix B. Supplementary data

Supplementary data associated with this article can be found in the online version at http://dx.doi.org/10.1016/j.epsl.2012.05.036.

References

Adriani, O., Barbarino, G.C., Bazilevskaya, X., et al., 2011. PAMELA measurements of cosmic-ray proton and Helium spectra. Science 332, 69–72.

Alanko-Huotari, K., Usoskin, I.G., Mursula, K., Kovaltsov, G.A., 2007. Cyclic variations of the heliospheric tilt angle and cosmic ray modulation. Adv. Space Res. 40, 1064–1069.

Alcaraz, J., Alpat, B., Ambrosi, G., et al., 2000a. Cosmic protons. Phys. Lett. B 490, 27–35.

Alcaraz, J., Alpat, B., Ambrosi, G., et al., 2000b. Helium in near Earth orbit. Phys. Lett. B 494, 193–202.

Bard, E., Raisbeck, G., Yiou, F., Jouzel, J., 1997. Solar modulation of cosmogenic nuclide production over the last millennium: comparison between ^{14}C and ^{10}Be records. Earth Planet. Sci. Lett. 150, 453–462.

Beer, J., 2000. Neutron monitor records in broader historical context. Space Sci. Rev. 93, 107–119.

Beer, J., McCracken, K., von Steiger, R., 2012. Cosmogenic Radionuclides: Theory and Applications in the Terrestrial and Space Environments. Springer, Berlin.

Bolin, B., Degens, E., Kempe, S., Ketner, P.E., 1979. The Global Carbon Cycle. John Wiley and Sons, New York.

Burger, R., Potgieter, M., Heber, B., 2000. Rigidity dependence of cosmic ray proton latitudinal gradients measured by the Ulysses spacecraft: implications for the diffusion tensor. J. Geophys. Res. 105, 27447–27456.

Castagnoli, G., Lal, D., 1980. Solar modulation effects in terrestrial production of Carbon-14. Radiocarbon 22, 133–158.

Clem, J.M., Bieber, J.W., Evenson, P., Hall, D., Humble, J.E., 1997. Contribution of obliquely incident particles to neutron monitor counting rate. J. Geophys. Res. 102, 26919–26926.

Damon, P., Sternberg, R., 1989. Global production and decay of radiocarbon. Radiocarbon 31, 697–703.

Dergachev, V., Veksler, V., 1991. Application of the Radiocarbon Method for Studies of the Environment in the Past. A.F. Ioffe Phys-Tech Inst., Acad. Sci. USSR, Leningrad, USSR (in Russian).

Desorgher, L., Flückiger, E.O., Gurtner, M., Moser, M.R., Bütikofer, R., 2005. Atmocosmics: a Geant 4 code for computing the interaction of cosmic rays with the Earth's atmosphere. Int. J. Mod. Phys. A 20, 6802–6804.

Dorman, L., 2004. Cosmic Rays in the Earth's Atmosphere and Underground. Kluwer Academic Publishers, Dordrecht, Netherlands.

Dorman, L., 2009. Cosmic Rays in Magnetospheres of the Earth and other Planets. Springer, New York.

Elsasser, W., Nay, E., Winkler, J., 1956. Cosmic-ray intensity and geomagnetism. Nature 178, 1226–1227.

Fermi, E., 2010. In: Esposito, S., Pisanti, O. (Eds.), Neutron Physics for Nuclear Reactions: Unpublished Writings by Enrico Fermi. World Scientific Publishing, Singapore.

Garcia-Munoz, M., Mason, G., Simpson, J., 1975. The anomalous ^{4}He component in the cosmic-ray spectrum at below approximately 50 MeV per nucleon during 1972–1974. Astrophys. J. 202, 265–275.

Geant4 Collaboration, Agostinelli, S., Allison, J., Amako, K., et al., 2003. Geant4—a simulation toolkit. Nucl. Instrum. Methods Phys. Res. A 506, 250–303.

Goslar, T., 2001. Absolute production of radiocarbon and the long-term trend of atmospheric radiocarbon. Radiocarbon 43, 743–749.

Heck, D., Knapp, J., Capdevielle, J., Schatz, G., Thouw, T., 1998. Corsika: a Monte Carlo code to simulate extensive air showers. In: FZKA 6019. Forschungszentrum, Karlsruhe.

Hedin, A.E., 1991. Extension of the MSIS thermosphere model into the middle and lower atmosphere. J. Geophys. Res. 96, 1159–1172.

Herbst, K., Kopp, A., Heber, B., Steinhilber, F., Fichtner, H., Scherer, K., Matthiä, D., 2010. On the importance of the local interstellar spectrum for the solar modulation parameter. J. Geophys. Res. 115, D00I20.

Hudson, H.S., 2010. Solar flares add up. Nat. Phys. 6 (9), 637–638.

Korff, S., Mendell, R., 1980. Variations in radiocarbon production in the Earth's atmosphere. Radiocarbon 22 (2), 159–165.

Korte, M., Constable, C., Donadini, F., Holme, R., 2011. Reconstructing the Holocene geomagnetic field. Earth Planet. Sci. Lett. 312, 497–505.

Kovaltsov, G.A., Usoskin, I.G., 2010. A new 3D numerical model of cosmogenic nuclide ^{10}Be production in the atmosphere. Earth Planet. Sci. Lett. 291, 182–188.

Kromer, B., 2009. Radiocarbon and dendrochronology. Dendrochronologia 27 (1), 15–19.

Lal, D., 1988. Theoretically expected variations in the terrestrial cosmic-ray production rates of isotopes. In: Cini Castagnoli, G. (Ed.), Solar-Terrestrial Relationships and the Earth Environment in the last Millennia, Proceedings of the International School of Physics "Enrico Fermi", Course XCV. North-Holland Publishing Company, Amsterdam, The Netherlands, pp. 216–233.

Lal, D., Suess, H., 1968. The radioactivity of the atmosphere and hydrosphere. Ann. Rev. Nucl. Sci. 18, 407–434.

LaViolette, P.A., 2011. Evidence for a solar flare cause of the pleistocene mass extinction. Radiocarbon 53 (2), 303–323.

Light, E.S., Merker, M., Verschell, H.J., Mendell, R.B., Korff, S.A., 1973. Time dependent worldwide distribution of atmospheric neutrons and of their products. 2. Calculation. J. Geophys. Res. 78, 2741–2762.

Lingenfelter, R., 1963. Production of carbon 14 by cosmic-ray neutrons. Rev. Geophys. Space Phys. 1, 35–55.

Lingenfelter, R., Ramaty, R., 1970. Astrophysical and geophysical variations in C-14 production. In: Olsson, I. (Ed.), Radiocarbon Variations and Absolute Chronology: Proceedings of the 12th Nobel Symposium. John Wiley & Sons, NY, pp. 513–537.

Lockwood, J.A., Webber, W.R., 1996. Comparison of the rigidity dependence of the 11-year cosmic ray variation at the earth in two solar cycles of opposite magnetic polarity. J. Geophys. Res. 101 (October), 21573–21580.

Masarik, J., Beer, J., 1999. Simulation of particle fluxes and cosmogenic nuclide production in the Earth's atmosphere. J. Geophys. Res. 104, 12099–12111.

Masarik, J., Beer, J., 2009. An updated simulation of particle fluxes and cosmogenic nuclide production in the Earth's atmosphere. J. Geophys. Res. 114, D11103.

Masarik, J., Reedy, R.C., 1995. Terrestrial cosmogenic-nuclide production systematics calculated from numerical simulations. Earth Planet. Sci. Lett. 136, 381–395.

McCracken, K., McDonald, F., Beer, J., Raisbeck, G., Yiou, F., 2004. A phenomenological study of the long-term cosmic ray modulation, 850–1958 AD. J. Geophys. Res. 109 (A18), 12103.

Muscheler, R., Joos, F., Beer, J., Müller, S., Vonmoos, M., Snowball, I., 2007. Solar activity during the last 1000 yr inferred from radionuclide records. Quat. Sci. Rev. 26, 82–97.

Nakamura, K., Hagiwara, K., Hikasa, K., et al., 2010. Review of particle physics. J. Phys. G 37 (7A), 1–1422.

O'Brien, K., 1979. Secular variations in the production of cosmogenic isotopes in the Earth's atmosphere. J. Geophys. Res. 84, 423–431.

O'Brien, K., 2008. Limitations of the use of the vertical cut-off to calculate cosmic-ray propagation in the Earth's atmosphere. Radiat. Prot. Dosimetry 128, 259–260.

O'Brien, K., 2010. The local all-particle cosmic-ray spectrum. Astrophys. J. 716, 544–549.

O'Brien, K., de la Zerda Lerner, A., Shea, M.D.F.S., 1991. The production of cosmogenic isotopes in the Earth's atmosphere and their inventories. In: Sonett, C., Giampapa, M., Matthews, M. (Eds.), The Sun in Time. University of Arizona Press, Tucson, USA, pp. 317–342.

Picone, J.M., Hedin, A.E., Drob, D.P., Aikin, A.C., 2002. NRLMSISE-00 empirical model of the atmosphere: statistical comparisons and scientific issues. J. Geophys. Res. 107. (Cite ID 1468).

Reimer, P.J., Baillie, M.G.L., Bard, E., et al., 2009. INTCAL09 and Marine09 radiocarbon age calibration curves, 0–50000 years cal BP. Radiocarbon 51 (4), 1111–1150.

Simpson, J.A., 1983. Elemental and isotopic composition of the galactic cosmic rays. Annu. Rev. Nucl. Part. Sci. 33, 323–382.

Snowball, I., Muscheler, R., 2007. Palaeomagnetic intensity data: an Achilles heel of solar activity reconstructions. Holocene 17, 851–859.

Solanki, S., Usoskin, I., Kromer, B., Schüssler, M., Beer, J., 2004. Unusual activity of the sun during recent decades compared to the previous 11,000 years. Nature 431, 1084–1087.

Steinhilber, F., Abreu, J.A., Beer, J., 2008. Solar modulation during the Holocene. Astrophys. Space Sci. Trans. 4, 1–6.

Stuiver, M., Braziunas, T., 1989. Atmospheric ^{14}C and century-scale solar oscillations. Nature 338, 405–408.

Stuiver, M., Quay, P., 1980. Changes in atmospheric Carbon-14 attributed to a variable sun. Science 207, 11–19.

Tylka, A., Dietrich, W., 2009. A new and comprehensive analysis of proton spectra in ground-level enhanced (GLE) solar particle events. In: 31th International Cosmic Ray Conference. Universal Academy Press, Lodź, Poland.

Usoskin, I., Kovaltsov, G., 2008. Production of cosmogenic ^{7}Be isotope in the atmosphere: full 3D modelling. J. Geophys. Res. 113.

Usoskin, I., Solanki, S., Kovaltsov, G., Beer, J., Kromer, B., 2006. Solar proton events in cosmogenic isotope data. Geophys. Res. Lett. 33, L08107.

Usoskin, I.G., Alanko-Huotari, K., Kovaltsov, G.A., Mursula, K., 2005. Heliospheric modulation of cosmic rays: monthly reconstruction for 1951–2004. J. Geophys. Res. 110, A12108.

Usoskin, I.G., Bazilevskaya, G.A., Kovaltsov, G.A., 2011. Solar modulation parameter for cosmic rays since 1936 reconstructed from ground-based neutron monitors and ionization chambers. J. Geophys. Res. 116, A022104.

Usoskin, I.G., Desorgher, L., Velinov, P., Storini, M., Flückiger, E.O., Bütikofer, R., Kovaltsov, G.A., 2009. Ionization of the Earth's atmosphere by solar and galactic cosmic rays. Acta Geophys. 57, 88–101.

Usoskin, I.G., Solanki, S.K., Kovaltsov, G.A., 2007. Grand minima and maxima of solar activity: new observational constraints. Astron. Astrophys. 471, 301–309.

Webber, W., Higbie, P., 2003. Production of cosmogenic Be nuclei in the Earth's atmosphere by cosmic rays: its dependence on solar modulation and the interstellar cosmic ray spectrum. J. Geophys. Res. 108, 1355.

Webber, W., Higbie, P., McCracken, K., 2007. Production of the cosmogenic isotopes ^{3}H, ^{7}Be, ^{10}Be and ^{36}Cl in the Earth's atmosphere by solar and galactic cosmic rays. J. Geophys. Res. 112.

Webber, W.R., Higbie, P.R., 2009. Galactic propagation of cosmic ray nuclei in a model with an increasing diffusion coefficient at low rigidities: a comparison of the new interstellar spectra with Voyager data in the outer heliosphere. J. Geophys. Res. 114, A02103.